

## Electrochemical and Theoretical Study of Metronidazole Drug as Inhibitor for Copper Corrosion in Hydrochloric Acid Solution

Adriana Samide<sup>1,\*</sup>, Bogdan Tutunaru<sup>1</sup>, Aurelian Dobrițescu<sup>1,\*</sup>, Petru Ilea<sup>2</sup>, Ana-Cristina Vladu<sup>1,2</sup>  
Cristian Tigae<sup>1</sup>

<sup>1</sup> University of Craiova, Faculty of Sciences, Department of Chemistry, Calea Bucuresti, 107i, Craiova, Romania

<sup>2</sup> Babes-Bolyai University, Faculty of Chemistry and Chemical Engineering, Department of Chemical Engineering, Arany Janos Street no. 11, Cluj-Napoca, Romania

\*E-mail: [samide\\_adriana@yahoo.com](mailto:samide_adriana@yahoo.com); [dobri\\_aur@yahoo.com](mailto:dobri_aur@yahoo.com)

Received: 3 April 2016 / Accepted: 17 May 2016 / Published: 4 June 2016

---

The approach current trend of expired drugs as corrosion inhibitors for metals and alloys in different environments to avoid its pollution with corrosion products by diminishing the degradation rate of materials is reflected, in our study, by investigation of metronidazole (MNZ) antibiotic and antiprotozoal drug, as corrosion inhibitor for copper in hydrochloric acid solution. The electrochemical measurements associated with UV-Vis spectrophotometry followed by quantum chemical calculations were performed, their results showing that: MNZ inhibition efficiency reached a value of 90.0 %  $\pm 2$ , at 1.0 mmol L<sup>-1</sup> inhibitor concentration; the amount of corrosion products decreases in the presence of MNZ; the formation of complexes between MNZ and copper, as well as their effective contribution to growth a protective layer at the metal/solution interface; MNZ action mechanism resulted from the parallel processes between the occurrence of chemical bonds and electrostatic interactions was certified by quantum chemical calculations, when *ab initio* to the approximate level of density functional theory (DFT) was used by assigning the Gamees molecular modeling.

---

**Keywords:** corrosion inhibition; metronidazole; electrochemical measurements; UV-Vis spectrophotometry; quantum chemical studies

### 1. INTRODUCTION

Copper and its alloys have been used in many types of industrial applications such as: materials for heat conductors/exchangers; electronic applications in communications; pipelines and electrical conductors due to their easy availability, the mechanical workability, high electrical and thermal

conductivities, low cost and relatively noble properties. Hydrochloric acid and other chloride environments can cause the corrosion of copper [1-5]. The electrochemical dissolution of copper in the presence of chloride anions occurs through  $\text{CuCl}$  and the formation of higher chloride complexes [6-10]. The anodic behaviour of copper in aqueous media of weakly acidic or at alkaline pH, has been also studied [11, 12], concluding that the corrosion products have a negative effect on its application.

Therefore, the copper corrosion inhibition has been extensively studied using the organic inhibitors which could effectively remove some destructive effects of environmental factors. The study of drugs, as a new class of friendly environmentally inhibitors, has gained much attention [13-17].

Streptoquin (4-amino-N-2-thiazolyl-N1-2-thiazolylsulfanilamide) and septazole (N1-(5-methyl-3-isoxazolyl) sulfanilamide) antibiotic drugs have been used as corrosion inhibitors for copper in  $0.1 \text{ mol L}^{-1}$  HCl solution [18, 19]. These drugs are physically adsorbed on copper surface acting as mixed-type inhibitors. The inhibition efficiencies of streptoquin and septazole, calculated from potentiodynamic polarization and electrochemical impedance spectroscopy reached the values of 80.9/88.6 % and 36.6/64.9 %, respectively, at their concentration of 700 ppm.

Domperidone was intensively studied as inhibitor for copper by weight loss (WL), potentiodynamic polarization (PP), electrochemical impedance spectroscopy (EIS), scanning electron microscopy (SEM), atomic force microscopy (AFM), quantum chemical studies (QCC) and molecular dynamics (MD) calculation [20]. The experimental results indicated a maximum inhibition efficiency of 94.2 % in 3.5 % NaCl solution. Three pharmaceutical compounds: 6-chloro-1,1-dioxo-3,4-dihydro-2H-1,2,4-benzothiadiazine-7-sulfonamide (1); 1-((s)-3-mercapto-2-methyl propanoyl) pyrrolidine-2-carboxylic acid (2); 3-(2-methoxy phenoxy) propane 1,2-diol (3) are effective corrosion inhibitors for copper in  $2.0 \text{ mol L}^{-1}$   $\text{HNO}_3$  solution. The inhibition efficiency values of these compounds increases with their concentration increase from  $10^{-6} \text{ mol L}^{-1}$  to  $11 \cdot 10^{-6} \text{ mol L}^{-1}$ , their inhibition performance decreases as follows: (1) > (2) > (3) [21]. Levetiracetam is another drug used for inhibition copper corrosion in  $0.5 \text{ mol L}^{-1}$   $\text{HNO}_3$  solution. The adsorption process obeys Langmuir isotherm and the inhibition efficiency reached a maximum value of 94.9 %, at a drug concentration of 300 ppm [22].

In this study, the corrosion inhibition of copper in  $1.0 \text{ mol L}^{-1}$  HCl solution using metronidazole drug (MNZ), IUPAC name: 2-(2-methyl-5-nitro-1H-imidazol-1-yl)ethanol was investigated, taking into consideration the results obtained from the electrochemical measurements associated with UV-Vis spectrophotometry and the quantum chemical studies, as support for the confirmation of experimental data.

## 2. MATERIALS AND METHODS

### 2.1. Materials

The copper specimens (99.9 % purity from EcoRoof) with an active area of  $1.0 \text{ cm}^2$ , were used to investigate the metronidazole drug (analytical standard product - Merck), as corrosion inhibitor in hydrochloric acid solution (AR grade from Merck). Five concentrations of MNZ:  $0.2 \text{ mmol L}^{-1}$ ;  $0.4 \text{ mmol L}^{-1}$ ;  $0.6 \text{ mmol L}^{-1}$ ;  $0.8 \text{ mmol L}^{-1}$ ;  $1.0 \text{ mmol L}^{-1}$ , were used in  $1.0 \text{ mol L}^{-1}$  HCl solution to obtain the corrosive media, by the side of  $1.0 \text{ mol L}^{-1}$  HCl blank solution, in order to study the

electrochemical behaviour of copper. Before corrosion the copper plates were polished with sandpaper of different sizes, degreased with acetone and dried between two sheets of filter paper.

## 2.2. Electrochemical measurements

The potentiodynamic polarization was carried out, with the potential scan rate of  $1.0 \text{ mV s}^{-1}$ , from  $-1000 \text{ mV}$  to  $1000 \text{ mV}$ , for copper in  $1.0 \text{ mol L}^{-1}$  HCl blank solution and in  $1.0 \text{ mol L}^{-1}$  HCl solution containing MNZ in various concentrations:  $0.2 \text{ mmol L}^{-1}$ ;  $0.4 \text{ mmol L}^{-1}$ ;  $0.6 \text{ mmol L}^{-1}$ ;  $0.8 \text{ mmol L}^{-1}$ ;  $1.0 \text{ mmol L}^{-1}$ , in order to determine the corrosion current density ( $i_{\text{corr}}$ ) and polarization resistance ( $R_p$ ) which were used to calculate the inhibition efficiency ( $IE\%$ ) of investigated inhibitor. The cyclic voltammetry was accomplished with a scan rate of  $100 \text{ mV s}^{-1}$ , at room temperature, from  $-1000 \text{ mV}$  to  $1000 \text{ mV}$ , on copper in  $1.0 \text{ mol L}^{-1}$  HCl solution containing MNZ in various concentrations:  $0.2 \text{ mmol L}^{-1}$ ;  $0.4 \text{ mmol L}^{-1}$ ;  $1.0 \text{ mmol L}^{-1}$ , the recorded voltammograms being compared to that obtained in blank solution.

The electrochemical measurements were conducted into an electrochemical cell with three electrodes, as follows: the working electrode manufactured from copper plates with an active area of  $1.0 \text{ cm}^2$ ; the auxiliary electrode was a platinum plate with the area of  $1.0 \text{ cm}^2$ ; the reference electrode of  $\text{Ag}/\text{AgCl}_{\text{sat}}$  was coupled by a Luggin capillary. An electrochemical system VoltaLab 40 with the VoltaMaster 4 software was used to perform the copper measurements in corrosive media mentioned above, at room temperature, the immersion time of the electrodes at open circuit, being of 4.0 minutes.

## 2.3. UV-Vis spectrophotometry

The acid blank solution with a concentration of  $1.0 \text{ mol L}^{-1}$  HCl and  $1.0 \text{ mol L}^{-1}$  HCl solution containing  $0.2 \text{ mmol L}^{-1}$  MNZ and  $0.4 \text{ mmol L}^{-1}$  MNZ were submitted for UV-Vis analysis before and after corrosion using an UV-Vis Varian-Cary 50 spectrophotometer with CaryWin software. The UV-Vis spectra, in wavelength range between 800 and 200 nm were recorded, and the absorbance maxima for corrosion products and metronidazole were highlighted.

## 2.4. Quantum chemical calculations

Quantitative assessment of the properties was done by *ab initio* quantum mechanical calculation at around the density functional theory, knowing as DFT method, with the assignment of the Gamees molecular modeling, with the input of MNZ molecule geometry that corresponds to the local minimum on a multidimensional area (hypersurface) of potential energy.

The calculation of the molecule geometry in the fundamental state of singlet, the electronic structure and molecule total energy, was based on hybrid model of change-correlation functional, B3LYP (Becke 3 Lee Yang Parr) that expresses the contribution of change-correlation energies resulted from the DFT formalism and the energy of change provided by Hartree-Fock models by

mixing Becke's functional of change with three parameters, with Lee-Yang-Parr's functional of correlation depending on  $\nabla^2\rho(r)$ .

### 3. RESULTS AND DISCUSSION

#### 3.1. Potentiodynamic polarization associated with UV-Vis spectrophotometry

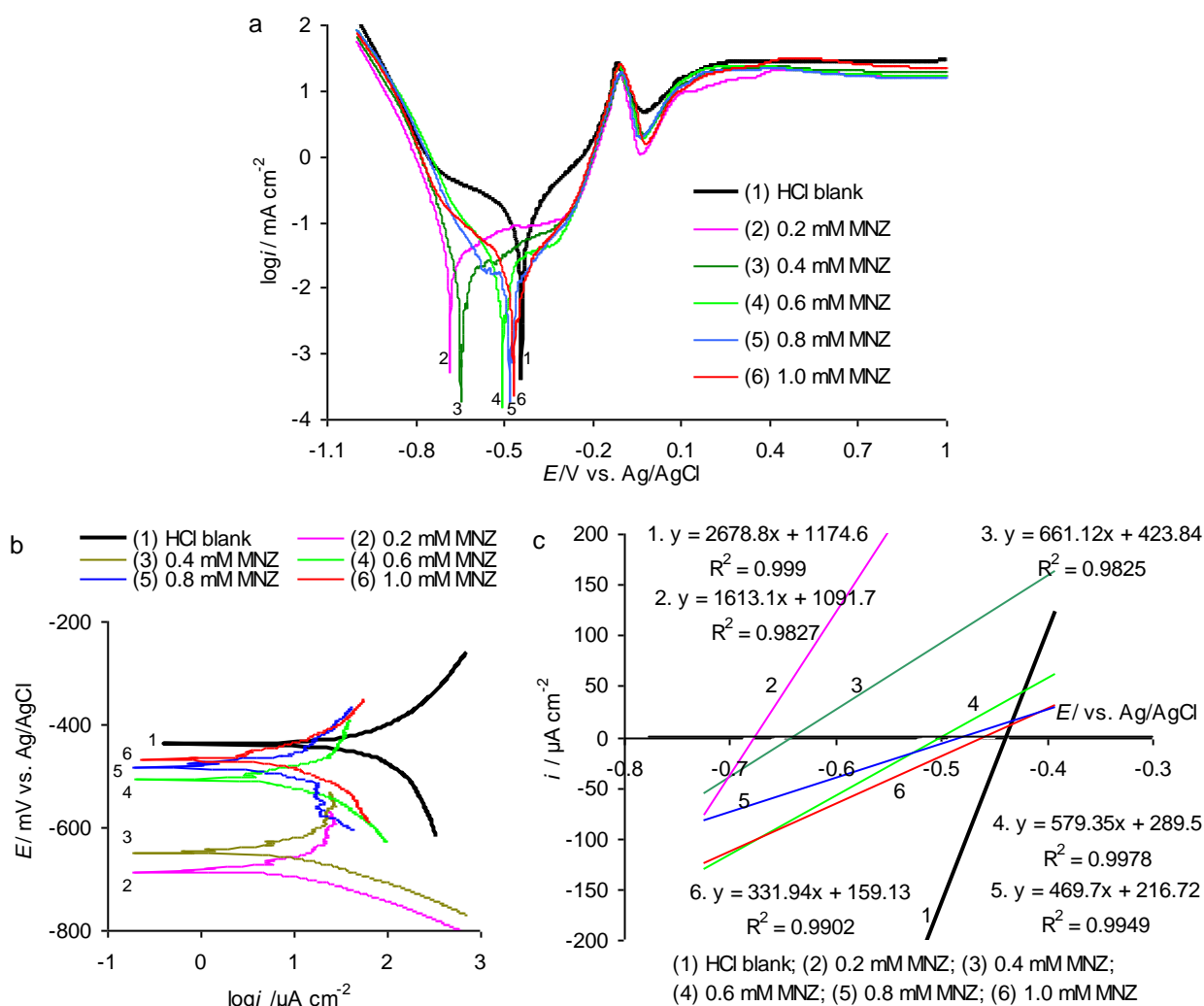


**Figure 1.** Potentiodynamic curves for copper in 1.0 mol L<sup>-1</sup> HCl solution, without and with MNZ, recorded: a – in the potential range from -1.0 V to 1.0 V; b – in the potential range of ± 200 mV around *E*<sub>corr</sub>; c – in the potential range of ± 20 mV around *E*<sub>corr</sub> illustrated as their tangent drawn to corrosion potential, *R*<sup>2</sup> values being close to unity

The results of potentiodynamic polarization are shown in Fig. 1. The potentiodynamic polarization curves recorded in the potential range, from -1.0 V to 1.0 V are presented in Fig. 1a, these expressing an overview on copper behavior in 1.0 mol L<sup>-1</sup> HCl solution in the absence and in the presence of metronidazole (MNZ). The addition of MNZ in 1.0 mol L<sup>-1</sup> HCl solution leads to: (i) the shifting of polarization curves in the lower current regions than that was recorded for blank solution; (ii) this leads to the decrease in the corrosion current density (*i*<sub>corr</sub>) depending on the MNZ

concentration; (iii) random movement of corrosion potential ( $E_{\text{corr}}$ ) in the negative direction, indicating that the addition of inhibitor can produce the change of environment composition, most likely due to the emergence of new species such as complexes of Cu(II) with MNZ and/or the occurrence of new compounds resulted from MNZ decomposition; (iv) the cathodic process is distinguished by linear polarization curves, in the potential range from -0.8 V to -1.0 V vs. Ag/AgCl<sub>sat</sub>, these are easily addicted of MNZ concentration; (v) in contrast, the polarization curves of anodic process present a passivation trend at -0.2 V vs. Ag/AgCl<sub>sat</sub>; after potential value of 0.15 V vs. Ag/AgCl<sub>sat</sub>, a plateau is observed, this being shifted to lower current density in the presence of MNZ in 1.0 mol L<sup>-1</sup> HCl solution.

To better explain the copper behavior in 1.0 mol L<sup>-1</sup> HCl blank solution and in 1.0 mol L<sup>-1</sup> HCl solution containing MNZ, the discussion on the active range of the polarization curves is necessary. Thus, the polarization curves were processed as Tafel and Stern diagrams, as shown in Figs. 1b and 1c. From Fig. 1b it can be seen that the MNZ adding leads to more pronounced displacement of polarization curves in negative direction with decrease in inhibitor concentration, but in lower current areas while the MNZ concentration increases. Consequently, the corrosion current density decreases with increase in the inhibitor concentration. Fig. 1c presents the linear domain of polarization curves recorded, in potential range of  $\pm 20$  mV, from aside and another of  $E_{\text{corr}}$ .

The polarization resistance ( $R_p$ ) can be calculated using the Eq. 1 [23]. The slopes of the lines represent the polarization conductance ( $C_p$ ) expressed as  $(di/dE)_{E \rightarrow E_{\text{corr}}}$ , its decrease leading to the  $R_p$  increase. As shown the equations inserted in Fig. 1c, the slopes of the lines decrease with increase in MNZ concentration, consequently  $R_p$  increases proportionally with the inhibitor concentration [23].

$$1/R_p = (di/dE)_{E \rightarrow E_{\text{corr}}} \quad (1)$$

From the data above mentioned and from the position of polarization curves recorded in the MNZ presence in 1.0 mol L<sup>-1</sup> HCl solution compared to that was obtained in uninhibited solution, it is very difficult to estimate the action mechanism of MNZ. For this reason the UV-Vis spectrophotometry was applied on inhibited and uninhibited solution, before and after potentiodynamic polarization performed on the large potential range, from -1.0 V to 1.0 V (Fig. 2).

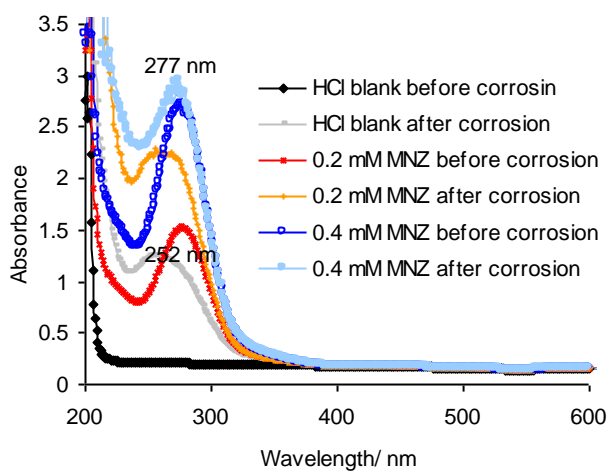


**Figure 2.** UV-Vis spectra recorded before and after potentiodynamic polarization for 1.0 mol L<sup>-1</sup> HCl blank solution and for 1.0 mol L<sup>-1</sup> HCl solution containing 0.2 mmol L<sup>-1</sup> and 0.4 mmol L<sup>-1</sup> MNZ

As illustrated in Fig. 2, peaks are not noted on the UV-Vis scan of uninhibited acid solution, before corrosion, in contrast with that was recorded after corrosion when a maximum at wavelength,  $\lambda_{\max} = 252$  nm is observed. This peak can be attributed to some corrosion products of  $\text{Cu}^+$  and  $\text{Cu}^{2+}$  which migrate in electrolyte, after corrosion [24, 25]. The modification of spectra according to the chloride concentration, as shown in early studies [24, 25], is a result of the consecutive replacement of water ligands with the chlorides ones. N. Zhang et al. [25] showed that the absorption band in the range of 230–320 nm may be attributed to some predictable compounds such as:  $\text{Cu}^{2+}$ ,  $[\text{CuCl}]^+$ ,  $[\text{CuCl}_2]^0$  and  $[\text{CuCl}_3]^-$ , and with the increase of  $\text{CuCl}_2$  concentration, a new absorption band appears centered at 385 nm. The copper corrosion in  $1.0 \text{ mol L}^{-1}$  HCl blank solution leads to the formation of copper corrosion products in low concentration, consequently an absorption band in the range of 230–320 nm was expected, it being observed in Fig. 2, at 252 nm [25].

In the presence of inhibitor in  $1.0 \text{ mol L}^{-1}$  HCl solution, before potentiodynamic polarization, the peak maximum, at  $\lambda_{\max} = 277$  nm is assigned to metronidazole that is in according to the literature data [26]. After corrosion, for both MNZ concentrations, the peak allure is noteworthy changed, but the wavelength of absorbance maximum is not altered, meaning that the interaction of MNZ with copper took place [26]. On the other hand, the absorption characteristics and the intensity of peak are changed due to the occurrence of new compounds, such as copper complexes with metronidazole [26, 27]. This statement is supported by the disappearance of the peak that corresponds to copper corrosion products scanned for uninhibited solution at 252 nm. It is clear that both, the strongly diminish of amount of copper corrosion products and the decrease of corrosion current density in the presence in MNZ, are due to the development of a protective layer on substrate surface, mainly due to the formation of complexes between copper and MNZ. Consequently, MNZ acts as corrosion inhibitor for copper in  $1.0 \text{ mol L}^{-1}$  HCl solution *via* complexes anchored on the substrate by adsorption that prevails the MNZ pure adsorption.

The electrochemical parameters listed in Table 1 were determined with VoltaMaster software that converted the corrosion current density ( $i_{\text{corr}}$ ) to corrosion rate (CR). The performance of MNZ as corrosion inhibitor for copper in  $1.0 \text{ mol L}^{-1}$  HCl solution was evaluated by the calculation of its inhibition efficiency (IE %) using the Eqs. 2 and 3 [1, 18, 21, 28].

$$IE = \frac{i_{\text{corr}}^{\circ} - i_{\text{corr}}}{i_{\text{corr}}^{\circ}} \times 100 \quad (2)$$

$$IE = \frac{R_p - R_p^{\circ}}{R_p} \times 100 \quad (3)$$

where:  $i_{\text{corr}}^{\circ}$  and  $R_p^{\circ}$  are the corrosion current density and polarization resistance obtained for the corrosion of copper in  $1.0 \text{ M}$  HCl uninhibited solution;  $i_{\text{corr}}$  and  $R_p$  are the corrosion current density and polarization resistance obtained for the corrosion of copper in  $1.0 \text{ M}$  HCl solution containing various concentrations of metronidazole.

The corrosion current density was calculated at intersection of Tafel lines to corrosion potential value; the polarization resistance was determined as mentioned above.

According to other studies related to the copper corrosion inhibition [1, 14-16, 18-22, 29], classical comments about data presented in Table 1, can be stipulated, as follows: (i) the increase in MNZ concentration leads to the decrease of corrosion current density ( $i_{\text{corr}}$ ) and corrosion rate ( $CR/\mu\text{m year}^{-1}$ ) while the increase of polarization resistance ( $R_p$ ) was obtained; the inhibition efficiency ( $IE$  %) becomes higher along with MNZ concentration increase, reaching an average value of  $90.0\% \pm 2$ , at  $1.0\text{ mmol L}^{-1}$  inhibitor in  $1.0\text{ M HCl}$  solution; (iii) the Tafel slopes are slightly changed suggesting that the corrosion inhibition takes place by blocking the active sites on copper surface, in this case preferentially by the adsorption of its complexes with MNZ.

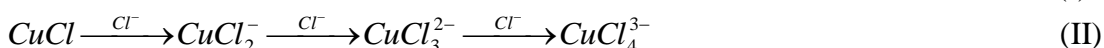
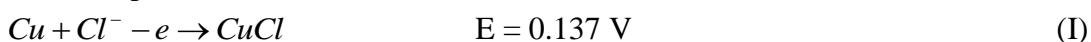
**Table 1.** The electrochemical parameters obtained for copper corrosion in  $1.0\text{ M HCl}$  solution, without and with various concentrations of MNZ, at room temperature; the inhibition efficiency ( $IE$  %) deduced from Tafel and using the polarization resistance ( $R_p$ ) values

C-MNZ/ $\text{mmol L}^{-1}$	$E_{\text{corr}}/$ $\text{mV vs.}$ $\text{Ag/AgCl}$	$i_{\text{corr}}/$ $\mu\text{A cm}^{-2}$	$b_a/$ $\text{mV dec}^{-1}$	$b_c/$ $\text{mV dec}^{-1}$	$CR/$ $\mu\text{m year}^{-1}$	$R_p/$ $\Omega\text{ cm}^2$	$IE/ \%$	
							from Tafel	from $R_p$
0	-439.0	125.8	123.0	-111.5	1519.0	373.3	-	-
0.2	-683.5	57.9	121.5	-116.1	699.2	619.9	53.9	39.8
0.4	-649.0	41.6	118.9	-126.3	502.3	1512.1	66.9	75.3
0.6	-506.5	32.4	130.1	-141.6	391.2	1726.1	74.2	78.4
0.8	-482.5	16.8	126.4	-131.4	202.6	2129.0	86.6	82.5
1.0	-469.0	10.3	132.4	-123.5	124.4	3012.6	91.8	87.6

### 3.2. Cyclic voltammetry

The electrochemical behaviour of the Cu electrode in  $1.0\text{ mol L}^{-1}\text{ HCl}$  solution, in the absence and in the presence of various concentrations of MNZ, has been investigated by cyclic voltammetry (CV). The voltammograms shown in Fig. 3 was recorded with a scan rate of  $100\text{ mV s}^{-1}$ , at room temperature.

Starting with an initial anodic scan, it can be seen the broad oxidation peaks (O1 and O2) registered in the potentials range  $-0.1 \div 0.4\text{ V}$  related to successive oxidation processes on copper surface (Fig. 3a) in the absence of metronidazole. At chloride anions concentration of  $1.0\text{ mol L}^{-1}$ , the copper dissolution occurs at working potential values around  $0.0\text{ V}$  through the formation of  $\text{CuCl}$  (O1; reaction I) [9, 18].  $\text{CuCl}$ , being sparingly soluble in water, reacts with  $\text{Cl}^-$  with the formation of several chloride species such as:  $\text{CuCl}_2^-$ ,  $\text{CuCl}_3^{2-}$  and  $\text{CuCl}_4^{3-}$  (reaction II) [29-31].



The chloride species present a strong interaction with copper substrate leading to a significant change in the surface morphology [32].

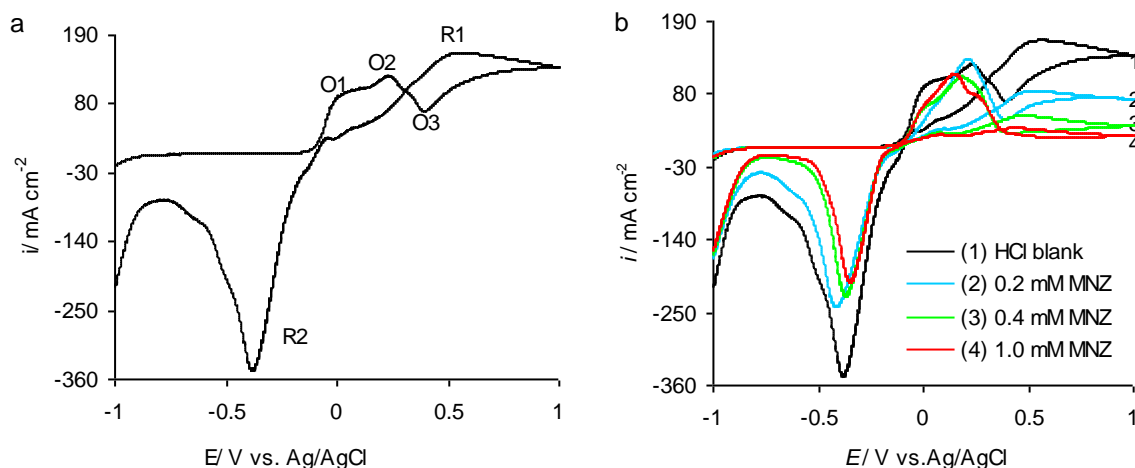


**Figure 3.** The cyclic voltammetry scans registered on copper in 1.0 mol L<sup>-1</sup> HCl solution in the absence of MNZ (a) and in 1.0 mol L<sup>-1</sup> HCl solution without and with MNZ (b)

The Cu<sup>+</sup> ions give further oxidation reactions on copper surface (peak O2) followed by their transformation in soluble cupric ions, as can be seen from reaction III [9].



At higher values of anodic potentials (~ 0.4 V), copper atoms are oxidized to Cu<sup>2+</sup> ions (peak O3 and reaction IV) [33]. The gradually increase of current densities, at higher potentials then 0.5 V, could be attributed to the oxidative copper dissolution reactions (reactions V and VI).



In the reverse scan, a hardly noticed peak (R1) is recorded at 0.15 V and is due to the reduction of CuCl adsorbed species. On further cathodic polarization of the copper electrode, the reduction peak R2 is assigned to the reduction of Cu<sup>+</sup>-chloride complexes [33]. From Fig. 3a, it can be concluded that at higher values of working potentials, copper preferably dissolved as soluble Cu<sup>2+</sup> species and the proportion Cu<sup>+</sup> species is reduced.

In the presence of MNZ (Fig. 3b), major changes can be seen in the region of the anodic current densities. As a consequence, some features are noticeable on the anodic and cathodic scans: (i) a sharper peak, in the potential range from -0.1 V to 0.4 V; (ii) gradually decreasing of anodic current densities along with the MNZ concentration increase; (iii) the cathodic current densities corresponding to R1 peak were strongly diminished with the increase in MNZ concentration; (iv) the reducing of hysteresis loop to almost zero, for 1.0 mmol L<sup>-1</sup> MNZ. The changes commented above may be a consequence of appearance a new species which migrated in the electrolyte, and a part of these were adsorbed on copper surface. This suggests that, in the presence of inhibitor, the formation of stable complexes of Cu(II) with MNZ occurred [26, 34, 35]. These complexes are strongly adsorbed on metallic surface reducing the electrochemical generation rate of Cu<sup>+</sup>/Cu<sup>2+</sup> species.



By corroborating data obtained from potentiodynamic polarization, UV-Vis spectrophotometry and cyclic voltammetry, it can be concluded that MNZ behaves as effective corrosion inhibitor for copper in 1.0 mol L<sup>-1</sup> HCl solution acting by the adsorption of its complexes on substrate surface.

### 3.3. Quantum chemical calculations

The geometry optimization without symmetry restriction was done in Cartesian coordinates Hartree-Fock at the level of Restricted Hartree-Fock (RHF) by Quasi-Newton-Raphson procedure, QA (Quadratic Approximation) being the optimization algorithm that was used (Fig. 4).

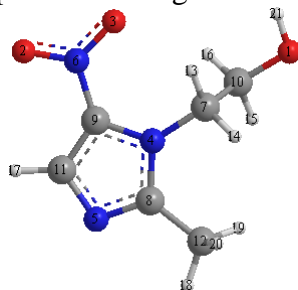


**Figure 4.** The optimized molecular structure of MNZ indicating the position of atoms, their color being: red – oxygen; blue – nitrogen; dark grey – carbon; light grey – hydrogen

It has taken into account the energy associated to the electrostatic interactions of metronidazole with water using Polarized Model Continuum (PMC) in the formulation version, IEF, (Integral Equation Formulation) [36]. The stationary point located on potential energy area was validated as local minimum by calculating of the vibration frequencies.

For greater flexibility of the form of atomic orbitals, it has used the basic expanded set 6-31G, by addition of the polarization functions which incorporate a higher kinetic momentum.

The adsorption of molecules on metal/electrolyte interface requires the existence of atoms with high electron density. These atoms act as electron donors to the vacant orbitals of metals.

The adsorption mechanism of metronidazole can be studied through the theory of frontier molecular orbitals, HOMO (Highest Occupied Molecular Orbital) and LUMO (Lowest unoccupied Molecular Orbital), because the interactions of donor-acceptor type between inhibitor molecules and metal surface are mediated by peripheral molecular orbitals: HOMO orbital of the inhibitor donates electrons to vacant low-energy LUMO orbital of the metal. The frontier molecular orbitals of MNZ are presented in Fig. 5.

The study of the area of the highest occupied molecular orbital, shows that the atomic orbitals from heterocyclic ring have the highest contribution, while the lowest unoccupied molecular orbital is distributed around -NO<sub>2</sub> group. Consequently, the heterocyclic ring has a greater tendency to donate electrons at the metal surface. From quantum-mechanical calculations the relevant molecular parameters are resulted, as follows:  $E_{\text{HOMO}} = -6.915$  eV;  $E_{\text{LUMO}} = -2.332$  eV; gap energy:  $\Delta E = E_{\text{LUMO}} - E_{\text{HOMO}} = 4.583$  eV.

The energy gap between HOMO and LUMO is an important molecular descriptor of chemical stability, meaning that a low value of this denotes a highly reactive molecule, suggesting that the electron density of the molecule can be easier changed, its resistance to charge transfer being smaller. The gap energy of 4.583 eV indicates a relatively high tendency of the inhibitor to form chemical bonds with the metal.

The values of the energy parameters of frontier molecular orbitals suggest that MNZ may act as a nucleophile, this having a greater tendency to donate the electrons than that of their acceptance [28].

The sum of energy of frontier molecular orbitals ( $E_{\text{LUMO}} + E_{\text{HOMO}}$ ) and the energy difference between them ( $E_{\text{LUMO}} - E_{\text{HOMO}}$ ) are correlated with the chemical reactivity of molecules *via* global quantum descriptors of reactivity: the absolute electronegativity ( $\lambda$ ) and absolute hardness ( $\eta$ ). Based on Koopmans and Janak's [37] theorems the absolute electronegativity and absolute hardness were calculated using the following relationships [28, 37]: Eqs. 4 and 5.

$$\lambda = -\frac{E_{\text{LUMO}} + E_{\text{HOMO}}}{2} \quad (4)$$

$$\eta = \frac{E_{\text{LUMO}} - E_{\text{HOMO}}}{2} \quad (5)$$

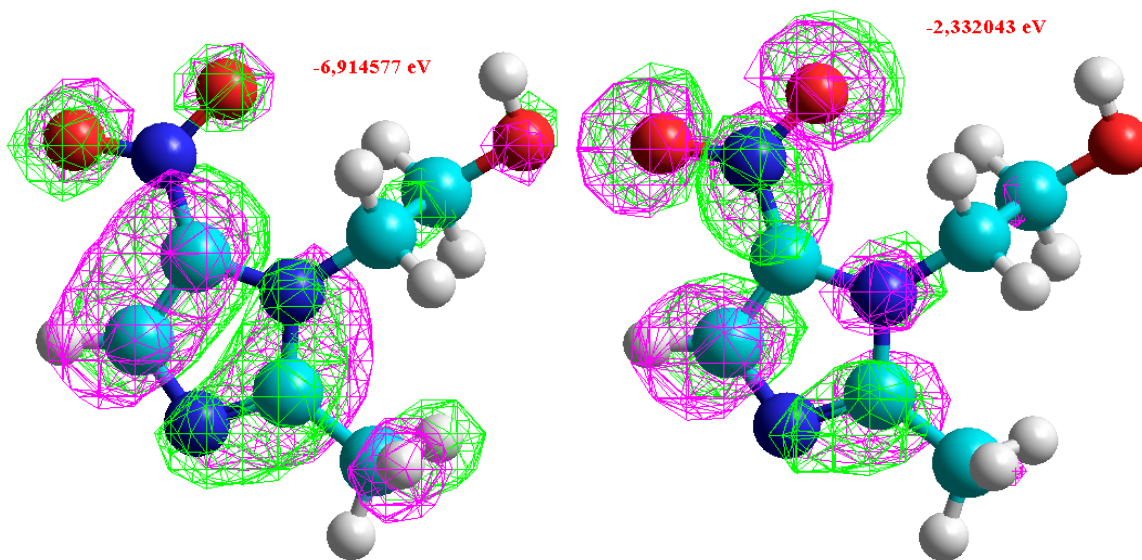


**Figure 5.** The frontier molecular orbitals: HOMO and LUMO

The absolute electronegativity ( $\lambda_{\text{MZN}}$ ) resulted from the calculation has a value of 4.623 eV, while the absolute hardness ( $\eta_{\text{MNZ}}$ ) reached 2.291 eV. The value of  $\lambda_{\text{MZN}}$  is smaller than the absolute electronegativity corresponding to copper from the volume phase ( $\lambda_{\text{Cu}} = 7.73$  eV) [38]. Therefore, the transfer of electrons takes place from metronidazole to copper.

The global softness ( $S$ ) is another parameter by which the quantum predictions of reactivity can be remarked. This is defined by Eq. 6 [37].

$$S = \frac{1}{2\eta} \quad (6)$$

The value obtained:  $S = 0.218$  eV, reveals that metronidazole is soft, that is consistent with its high polarizability.

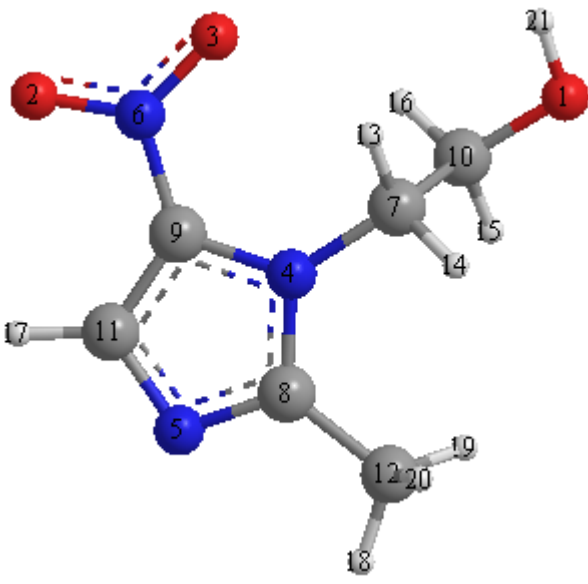
During the interaction between inhibitor and metal surface by chemical bonds, the fraction of the electrons transferred from metronidazole to copper ( $\Delta N$ ) was calculated with a similar formula to that from Pearson previous study [38], Eq. 7:

$$\Delta N = \frac{\lambda_{\text{Cu}} - \lambda_{\text{MZF}}}{2(\eta_{\text{Cu}} + \eta_{\text{MZF}})} \quad (7)$$

The value of  $\Delta N = 0.678$  indicates a great tendency of MNZ to donate electrons to vacant and/or vacanted orbitals of copper and/or copper(II) with the formation of the complexes.

The existence in the inhibitor molecule of several atoms with high negative partial charge determines the occurrence of a higher number of donor-acceptor interactions, therefore a better adsorption of MNZ to the metal/solution interface. Consequently, the theoretical study of the distribution way of the total electron density partitioned between atoms, may confirm or refute the hypothesis of the chemisorption capacity. Thus, in Table 2 are listed the Mulliken charges which were determined for MNZ.

**Table 2.** The atom charges obtained by analysis of Mulliken atomic populations

Optimized molecular structure of MNZ	Indexed atom	Mulliken atomic charges	Mulliken atomic populations
	<b>O(1)</b>	<b>-0.530117</b>	<b>8.53012</b>
	<b>O(2)</b>	<b>-0.39834</b>	<b>8.39834</b>
	<b>O(3)</b>	<b>-0.435915</b>	<b>8.43591</b>
	<b>N(4)</b>	<b>-0.491902</b>	<b>7.4919</b>
	<b>N(5)</b>	<b>-0.47533</b>	<b>7.47533</b>
	<b>N(6)</b>	0.336734	6.66327
	C(7)	-0.083306	6.08331
	C(8)	0.464161	5.53584
	C(9)	0.472813	5.52719
	C(10)	0.056861	5.94314
	C(11)	0.078067	5.92193
	C(12)	-0.389526	6.38953
	H(13)	0.147785	0.852215
	H(14)	0.129085	0.870915
	H(15)	0.113046	0.886954
	H(16)	0.116349	0.883651
	H(17)	0.136098	0.863902
	H(18)	0.159506	0.840494
	H(19)	0.136693	0.863307
	H(20)	0.1405	0.8595
	H(21)	0.316741	0.683259

The data listed in Table 2 regarding the partial charges of the atoms in MNZ molecule resulted from Mulliken partitioning scheme, show the existence of several atoms with a great tendency to donate electrons to metal surface: O(1), O(2), O(3), N(4) și N(5).

Therefore, it may be presumed the chemical interactions of metronidazole with metal surface are possible by these adsorption centers, which is why it can be affirmed that it supports the hypothesis of a chemical adsorption.

The Mulliken charges have lower values for the oxygen atoms from -OH and -NO<sub>2</sub> groups and for the nitrogen atoms from heterocyclic ring, as shown in Table 2 and Fig. 6 that illustrate the distribution map of Mulliken charges.

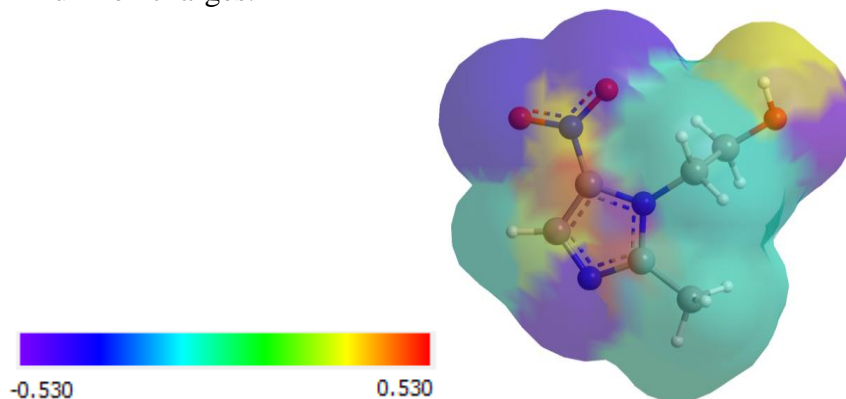


**Figure 6.** The Mulliken charges mapped on molecular surface that is accessible to solvent

Another molecular parameter resulted from quantum chemical calculations is the electric dipole moment ( $\mu$ ) that reflects the partial separation of the electric charge, in the molecule. This descriptor of the molecule polarity, also represents a predictor of chemical reactivity of molecules. Its value of 3.364 D suggests a good adsorption capacity of polar metronidazole molecules on the metal surface.

It should be emphasized that the real distribution of electron density in the metronidazole molecule is proved by the high value of the electric dipole moment resulted from quantum-chemical calculations ( $\mu = 3.364$  D). The chemical interactions between metronidazole and copper surface are duplicated by the electrostatic interactions between inhibitor atoms having the high positive partial charges (Fig. 6) and the chloride anions.

The interaction between the metronidazole and the metal surface mediated by chemical bonds is only possible for a certain form of the molecule (determined by the geometry of the atomic nucleus) and an electron density distribution in molecule that generates electron-rich regions.

Based on the molecular property as the molecular electrostatic potential it was obtained the 3D map of electron density. The molecular electrostatic potential sign and its amplitude make the difference between electron-rich regions and electron-poor regions. The different values of molecular electrostatic potential, marked by various colors, are mapped over an isodensity area of 0.002 electrons /a.u. (Fig. 7).

3D graphical model, that shows the spatial distribution of electrons in the metronidazole molecule, highlights: (i) the size of the metronidazole molecule and its form, which exclude the steric hindrance, cause a better adsorption on the metal surface and the greater its coverage; (ii) the adsorbed

molecules of inhibitor are oriented approximately parallel to the metal surface leading to the maximization of the number of contact points; (iii) there are reactive centers on the molecular surface which correspond to the most negative values of the molecular electrostatic potential (marked with blue) and these are adjacent to the oxygen atoms and unbound nitrogen (N5) atom from the heterocyclic ring.

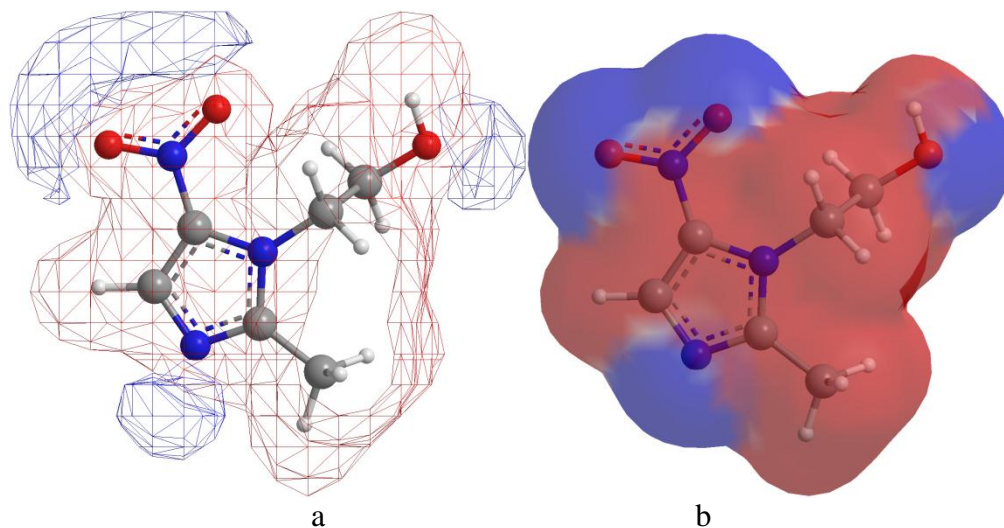


**Figure 7.** The surface of molecular electrostatic potential (a); the molecular electrostatic potential mapped on the area of charge total density (b)

#### 4. CONCLUSIONS

To elucidate the MNZ performance as corrosion inhibitor for copper in  $1.0 \text{ mol L}^{-1}$  HCl solution the potentiodynamic polarization and the cyclic voltammetry were performed at room temperature, in static regime. The UV-Vis spectra were obtained for aggressive media without and with inhibitor to detect the amount of corrosion products before and after potentiodynamic polarization, in order to discuss the MNZ action mechanism. The quantum chemical studies were reported as the support of electrochemical experimental data.

According to the electrochemical measurements metronidazole behaves as effective corrosion inhibitor for copper in  $1.0 \text{ mol L}^{-1}$  HCl solution, its inhibition efficiency reached a value of  $90.0 \pm 2\%$ , at  $1.0 \text{ mmol L}^{-1}$  inhibitor concentration.

The UV-Vis spectrophotometry confirms the decrease of amount of corrosion products, in the presence of inhibitor and the change in MNZ peak allure, after corrosion without altering of wavelength, indicating the MNZ-copper complexes appearance, this being the support for the action mechanism discussion regarding the protective layer formation at metal/solution interface that prevails other electrostatic interactions.

The cyclic voltammetry is in good agreement with those discussed above confirming the influence of MNZ on copper oxidation process.

The quantum chemical calculation took into account the theory of frontier molecular orbitals, HOMO and LUMO and several quantum descriptors of reactivity: the absolute electronegativity ( $\lambda$ ) and absolute hardness ( $\eta$ ), as well as the electric dipole moment ( $\mu$ ). The partial charges of the atoms in MNZ molecule resulted from Mulliken partitioning scheme were commented and the molecular electrostatic potential mapped on the surface of charge total density was displayed. All these sustain the affirmation that the chemical bonds between copper and MNZ were formed and consequently, the action mechanism *via* its complexes is confirmed, but the electrostatic interactions are possible through „bridged chloride”.

## References

1. K. Rhattas, M. Benmessaoud, M. Doubi, N. Hajjaji and A. Srhiri, *Mater. Sci. Appl.*, 2 (2011) 220.
2. E. M. Sherif, R. M. Erasmus and J. D. Comins, *J. Colloid. Interf. Sci.*, 309 (2007) 470.
3. H. Otmacic, J. Telegdi, K. Papp and E. Stupnisek-Usac, *J. Appl. Electrochem.*, 34 (2004) 545.
4. El-Sayed M. Sherif, *Int. J. Electrochem. Sci.*, 7 (2012) 1884.
5. L. Nunèz, E. Reguera, F. Corvo, F. Gonzalez and C. Vazquez, *Corros. Sci.*, 47 (2005) 461.
6. M. A. Malik, M. A. Hashim, F. Nabi, S. A. AL-Thabaiti and Z. Khan, *Int. J. Electrochem. Sci.*, 6 (2011) 1927.
7. D. Giménez-Romero, C. Gabrielli, J. J. García-Jareño, H. Perrot and F. Vicente, *J. Electrochem. Soc.*, 153 (2006) J32.
8. El-Sayed M. Sherif and A. A. Almajid, *J. Appl. Electrochem.*, 40 (2010) 1555.
9. A. El-Warraky, H. A. El-Shayeb and E. M. Sherif, *Anti-Corros. Method M.*, 51 (2004) 52.
10. M. M. Antonijevic, S. C. Alagic, M. B. Petrovic, M. B. Radovanovic and A. T. Stamenkovic, *Int. J. Electrochem. Sci.*, 4 (2009) 516.
11. A. Naseer and A. Y. Khan, *Turk. J. Chem.*, 34 (2010) 815.
12. A. Naseer, and A. Y. Khan, *Turk. J. Chem.*, 33 (2009) 739.
13. D. Q. Zhanga, Q. R. Cai, X. M. He, L. X. Gao and G. S. Kim, *Mater. Chem. Phys.*, 114 (2009) 612.
14. K. Barouni, M. Mihit, L. Bazzi, R. Salghi, S.S. Al-Deyab, B. Hammouti and A. Albourine, *The Open Corrosion Journal*, 3 (2010) 58.
15. D. Q. Zhang, L. X. Gao and G. D. Zhou, *J. Appl. Electrochem.*, 35 (2005) 1081.
16. K. Barouni, L. Bazzi, R. Salghi, M. Mihit, B. Hammouti, A. Albourine and S. El Issami, *Mater. Lett.*, 62 (2008) 3325.
17. J. B. Matos, L. P. Pereira, M. S. L. Agostinho, O. E. Barcia, G. G. O. Cordeiro and E. D'Elia, *J. Electroanal. Chem.*, 570 (2004) 91.
18. A. S. Fouda and H. E. Gadow, *Global J. Res. Eng.: C Chem. Eng.*, 14 (2014) 21.
19. A. S. Fouda, M.N. EL-Haddad and Y.M.Abdallah, *Int. J. Innov. Res. Sci., Eng. Technol.*, 2 (2013) 7073.
20. D. Wang, B. Xiang, Y. Liang, S. Song and C. Liu, *Corros. Sci.*, 85 (2014) 77.
21. A. M. Eldesoky, H. M. Hassan and A. S. Fouda, *Int. J. Electrochem. Sci.*, 8 (2013) 10376.
22. G. Karthik and M. Sundaravadivelu, *Egypt. J. Pet.* (2015)  
<http://dx.doi.org/10.1016/j.ejpe.2015.10.009>.
23. A. Samide, P. Rotaru, C. Ionescu, B. Tutunaru, A. Moanță and V. Barragan-Montero, *J. Therm. Anal. Calorim.*, 118 (2014) 651.
24. J. Brugger, D. C. McPhail, J. Black and L. Spiccia, *Geochim. Cosmochim. Acta*, 65 (2001) 2691.
25. N. Zhang, Q. Zhou, X. Yin and D. Zeng, *J. Solution. Chem.*, 43 (2014) 326.  
[DOI: 10.1007/s10953-014-0129-8](https://doi.org/10.1007/s10953-014-0129-8).

26. F. Siraji, A. T. M. Z. Azam, M. S. Amran, J. N. Islam, F. M. Amjad and M. A. Hossain, *J. Sci. Res.*, 4 (2012) 173.
27. J. A. Obaleye and A. Lawal, *J. Appl. Sci. Environ. Manage.*, 11 (2007) 15.
28. I. B. Obot, E. E. Ebenso and M. M. Kabanda, *J. Environ. Chem. Eng.*, 10 (2013) 431.
29. El-Sayed M. Sherif, *Int. J. Electrochem. Sci.*, 7 (2012) 1482.
30. C. Leger, F. Argoul and M. Bazant, *J. Phys. Chem. B*, 103 (1999) 5841.
31. S. M. Milic and M. M. Antonijevic, *Corros. Sci.*, 51 (2009) 28.
32. S. Huemann, N. T. M. Hai, P. Broekmann and K. Wandelt, *J. Phys. Chem. B*, 110 (2006) 24955.
33. A. K. Satpati and A. V. R. Reddy. *Int. J. Electrochem.*, 2011 (2011) ID 173462, <http://dx.doi.org/10.4061/2011/173462>.
34. F. Athar, K. Husain, M. Abid, S. M. Agarwal, S. J. Coles, M. B. Hursthouse, M. R. Maurya and A. Azam, *Chem. Biodivers.*, 2 (2005) 1320.
35. A. Lawal, J. A. Obaleye, S. A. Oyeleke and S. A. Amolegbe, *Centrepont (Science Edition)*, 15 (2009) 54.
36. J. Tomasi, B. Mennucci and R. Cammi, *Chem. Rev.*, 105 (2005) 2999.
37. J. Janak, *Phys. Rev. B*, 18 (1978) 7165.
38. R. G. Pearson, *Inorg. Chem.*, 27 (1988) 734.

© 2016 The Authors. Published by ESG ([www.electrochemsci.org](http://www.electrochemsci.org)). This article is an open access article distributed under the terms and conditions of the Creative Commons Attribution license (<http://creativecommons.org/licenses/by/4.0/>).